Journal of Statistical Physics, Vol. 89, Nos. 1/2, 1997

Vibrations of Simple Fractal-Based Models

John C. Kimball[1] and Harry L. Frisch[2]

Received June 20, 1996; final October 30, 1996

Dynamical systems with fractal geometry can be constructed in a variety of ways. We illustrate this variety with examples based on the Cantor set, the Sierpinski gasket, and on lattices of these fractal-based structures. Depending on the physical parameters, the models can exhibit both discrete and continuous spectra.

KEY WORDS: Fractal; lattice vibration; Cantor set; Sierpinski gasket.

1. INTRODUCTION

Although a fractal is often considered to be only a geometric object, it can be endowed with properties which turn it into a model physical system.[1] In particular, by placing masses and springs on a fractal, one can study the vibrations of systems with fractal geometry. There are many ways to decorate a fractal with masses and springs, and different choices correspond to different physics. For example, studies of fractal arrays in which every mass and every spring is the same have been used to model a variety of physical systems, including percolating networks and aerogels.[2] However, in other real systems (like trees or snowflakes), the finer portions of the fractal-like structure will have smaller masses, effective spring constants will vary with the scale, and the elastic couplings may be long ranged. As a first attempt to see the effects of non-uniform mass and spring-constant distributions, we consider two specially simple examples with varying masses and spring constants. In these examples, the masses become increasingly small as one looks at the fractal-based models on ever finer scales. The elastic couplings also scale with size, and (in the second example) the coupling are long ranged. In order to clearly demonstrate the

[1] Department of Physics, University at Albany, Albany, New York 12222.
[2] Department of Chemistry, University at Albany, Albany, New York 12222.

0022-4715/97/1000-0453$12.50/0

types of vibrations which result from variable masses, we have chosen solvability and simplicity over realism. Thus the examples presented here are only fanciful models of trees and snowflakes.

Our first model is one-dimensional and is related to the Cantor set. The second is two-dimensional and is roughly related to the Sierpinski gasket. These models are examples of a much broader class of systems which are neither periodic nor random. Many of the solved members of this class are one-dimensional. For example, models related to the Fibonacci sequence, introduced by Kohmoto *et al.*,[3] and by Ostlund *et al.*[4] have attracted considerable interest and applications.[5, 6, 7, 8, 9, 10] Such systems can have singular continuous spectra.[11] Another non-periodic but ordered one-dimensional model was introduced by Keirstead *et al.*,[12] and a model related to the Koch curve was described by Kappertz *et al.*[13] Also, physical experiments on the vibrations of a real system with Cantor-set geometry and an underlying mass hierarchy have been reported recently.[14] Our first example has some similarities to this physical system, but there are also significant differences.

In two (or more) dimensions, several previous vibration studies have been based on the Sierpinski gasket. Specially important results by Rammal[15] and Domany *et al.*[16] described the normal modes of a Sierpinski gasket with identical masses at each vertex and identical springs connecting nearest-neighbor masses. They showed that this system has a complete set of "super-localized" normal modes. They also showed that each normal mode frequency is infinitely degenerate, and the spectrum (normal mode frequencies plus limit-point frequencies) is a Julia set. Related numerical work[17, 18] and alternative results[19] have also been reported for this model. Another vibration model related to the Sierpinski gasket, which incorporated vector displacements, was introduced by Bergman *et al.*[20] There are some results for other fractal-based models[21, 22] specially the Vicsek fractal.[23, 24] Our two-dimensional example is quite different from the Sierpinski gasket examples cited above because our model has an infinite number of springs connected to each site. These multiple connections have some relation to a special Potts model on a Sierpinski gasket structure described by de Menezes *et al.*.[25] Because our Sierpinski gasket model has springs which extend across the entire gasket, it is no surprise that the normal modes we obtained are always different from the "super-localized" normal modes of the lattice described by Domany *et al.* and Rammal.

Our one-dimensional and two-dimensional examples are both constructed so the self-similarity of the underlying fractal is reflected in the vibrations. When either example is viewed on a smaller scale, its dynamics are nearly the same—except the characteristic frequency is changed by a

frequency-scaling parameter, η. Important properties of both examples are determined by η. The simplicity of the models and the self-similarity of the underlying fractal structure allow us to derive recursion relations which relate the systems' response functions at a frequency ω to the response functions at the scaled frequency $\eta\omega$. When $\eta > 1$ and the total mass is finite, these recursion relations have solutions which imply very simple vibration spectra: the normal mode frequencies form a discrete, unbounded, non-degenerate set with no accumulation points. Numerical results which illustrate this case are presented for the one-dimensional example based on the Cantor set.

Our Cantor set example does not make physical sense when the characteristic frequencies are scale-independent ($\eta = 1$). However, our two-dimensional example related to the Sierpinski gasket can be constructed with $\eta = 1$. When $\eta = 1$ the recursion relations become simple algebraic equations, and they describe a continuous vibration spectrum which is totally different from the discrete spectrum obtained when $\eta > 1$ in either model.

2. CANTOR SET MODEL

We change the Cantor set into a vibration model by placing a spring in each of the open intervals which complement the Cantor set. A mass is placed at both ends of each spring and at the ends of the Cantor set. The second step in the construction of this model is shown in Fig. 1a. The spring in each removed interval of length $(1/3)^n$ has a spring constant $k\Gamma^{n-1}$ with $\Gamma > 1$. A mass m is at each end of the Cantor set, and the interior masses are $m\gamma^n$, where $\gamma < 1$ and n is the exponent characterizing the spring connected to the mass. Results presented in Figs. 2a, 3a are for $\Gamma = 3$ and $\gamma = 1/3$.

Characteristics of this decorated Cantor set are revealed by its linear response to external forces. If oscillatory forces with frequency ω and amplitudes F_L and F_R are applied to the left and right ends, the displacement amplitudes at the two ends, X_L and X_R, are related to the forces by an inverse linear-response matrix;

$$\begin{pmatrix} F_L \\ F_R \end{pmatrix} = \begin{pmatrix} A(\omega) - m\omega^2 & B(\omega) \\ B(\omega) & A(\omega) - m\omega^2 \end{pmatrix} \begin{pmatrix} X_L \\ X_R \end{pmatrix}. \tag{1}$$

The forces needed to move only the end masses ($-m\omega^2 X_L$ and $-m\omega^2 X_R$) have been separated out, so the "response functions" $A(\omega)$ and $B(\omega)$ characterize the forces needed to move the internal coordinates of

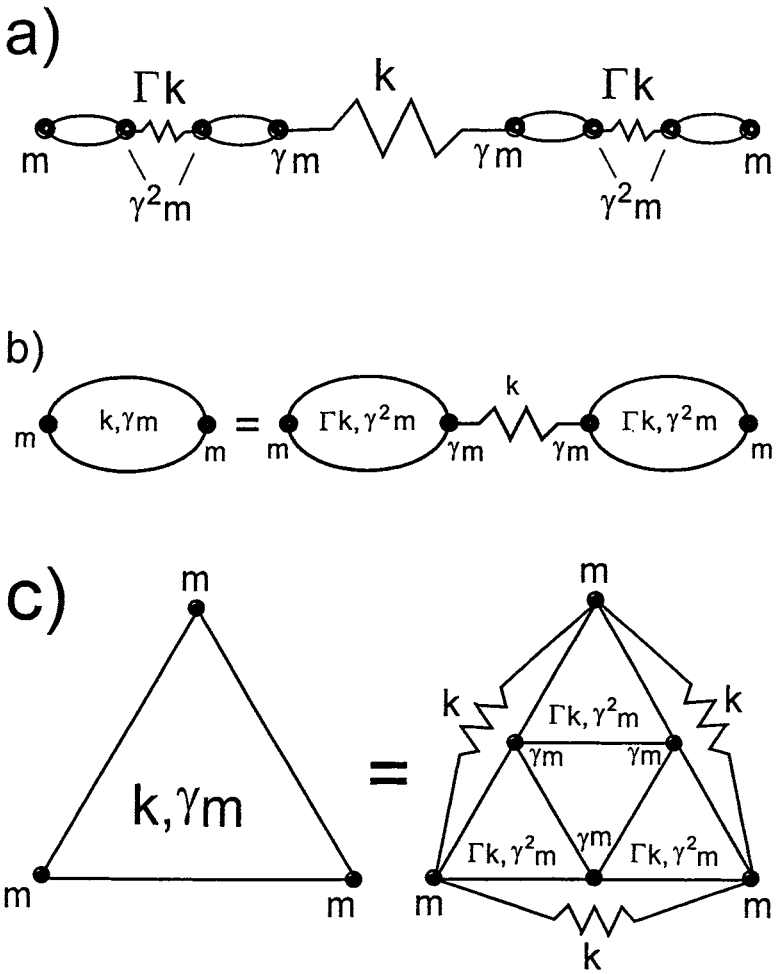

Fig. 1. (a) A system of masses and springs related to the geometry of the Cantor set. Further iterations insert additional springs into the intervals enclosed by the "lens" shapes. (b): A diagrammatic representation of the iteration used to construct the decorated Cantor set. (c): A diagrammatic representation of the iteration used to construct the fractal model related to the Sierpinski gasket.

the Cantor set. Normal modes of this system (with fixed end-points) correspond to poles in the response functions.

The springs and masses placed on the Cantor set extend its geometric self-similarity to the dynamic self-similarity which is illustrated in Fig. 1b. The "Cantor subset" composed of the left-hand third of the decorated Cantor set is identical to the original model, except each spring constant is

increased by Γ and each mass (except the left end-point mass) is decreased by γ. The linear response of the Cantor subset is similarly characterized. The force and displacement amplitudes on the left end are again denoted F_L and X_L, and the force and displacement amplitudes at the other end are denoted f_R and x_R. Then

$$\begin{pmatrix} F_L \\ f_R \end{pmatrix} = \begin{pmatrix} a(\omega) - m\omega^2 & b(\omega) \\ b(\omega) & a(\omega) - \gamma m\omega^2 \end{pmatrix} \begin{pmatrix} X_L \\ x_R \end{pmatrix}. \tag{2}$$

As before, the end-point mass contributions have been written separately. This means the response functions characterizing the Cantor set and the Cantor subset are exactly related by a scaling of the frequency and a multiplicative factor. Characteristic frequencies are the square roots of a spring-constant-to-mass ratio, so frequencies in the Cantor subset are scaled by

$$\eta = \sqrt{\frac{\Gamma}{\gamma}}. \tag{3}$$

Also the ratio of forces to displacements is proportional to a spring constant. Thus scaling means

$$a(\eta\omega) = \Gamma A(\omega); \qquad b(\eta\omega) = \Gamma B(\omega). \tag{4}$$

The reflection symmetry of the Cantor set and the scaling relations yield recursion relations for the response functions. First consider the reflection-symmetric "translation-like" motion which corresponds to $X_L = X_R$, and $F_L = F_R$. Symmetry means the translation-like modes of the Cantor set leave the center spring undisturbed, so $f_R = 0$. Using this condition and equating the ratio F_L/X_L obtained from Eq. (1) and from Eq. (2) gives

$$A(\omega) + B(\omega) = a(\omega) - \frac{(b(\omega))^2}{a(\omega) - \gamma m\omega^2}. \tag{5}$$

Replacing ω with $\eta\omega$, and using the scaling relations of Eq. (4) gives the first of two recursion relations for the response functions;

$$A(\eta\omega) + B(\eta\omega) = \Gamma\left(A(\omega) - \frac{(B(\omega))^2}{A(\omega) - m\omega^2}\right). \tag{6}$$

The second recursion relation is obtained by considering the "compression-like" motion which corresponds to $X_L = -X_R$ and $F_L = -F_R$. For this case, the center spring is symmetrically compressed, so $f_R = -2kx_R$. Again

equating the ratio F_L/X_L as given by the two response matrices, and using the scaling relations gives

$$A(\eta\omega) - B(\eta\omega) = \Gamma\left(A(\omega) - \frac{(B(\omega))^2}{A(\omega) + 2k/\Gamma - m\omega^2}\right). \tag{7}$$

The recursion relations of Eqs. (6), (7) are a central result from which a number of physical conclusion can be obtained. The linear response functions illustrated in Fig. 2a, the power-law of Eq. (9), and other observation about the distribution of the normal modes all follow from these equations. However, these conclusion are valid only if $\gamma < 1/2$ and $\Gamma > 2$. As we show below, these restrictions on the model parameters are needed to insure that the response functions are relatively smooth and well-defined.

When $\gamma < 1/2$ the total mass of the model is finite. (Summing the appropriate geometric series gives this total mass as $M = m + m/(1-2\gamma)$.) Also, when $\Gamma > 2$ the end-to-end spring constant is non-zero. (The geometric sum of inverse spring constants gives $K = k(1-2/\Gamma)$.) For these restricted values for Γ and γ, $\omega_0 = \sqrt{K/M}$ is a lower bound for the normal mode frequencies. (Placing all the masses at the end of all the springs can only lower a normal-mode frequency.) For frequencies smaller than ω_0, the response functions will be smooth and bounded. Thus substituting an expansion of $A(\omega)$ and $B(\omega)$ (in powers of ω^2) into the recursion relations yields the low frequency behavior of the system. In particular, for $\omega = 0$ the recursion relations become algebraic conditions on the static response functions. Solving these equations (with the restriction that $A(0) > 0$ for mechanical stability) gives $A(0) = -B(0) = K$. As one would expect, these values characterize the static response of a spring with the end-to-end spring constant, K. To first order in ω^2, $A(\omega) \cong K + \alpha m\omega^2$ and $B(\omega) \cong -K + \beta m\omega^2$. Substituting these into (Eq. (6)) gives $A(\omega) + B(\omega) \to -(M/2 - m)\,\omega^2$. This is the result one expects; when $F_L = F_R$, each force accelerates half the total mass, M, but the end-point mass accelerations are listed separately in the response matrix.

Starting with the low-frequency power series, multiple iterations of the recursion relations yield the response functions at higher frequencies. In practice, one does this by picking a "seed frequency" $\Omega \ll \omega_0$ which is so small that $A(\Omega)$ and $B(\Omega)$ are accurately approximated by only the constant and Ω^2 terms in their expansions. Repeated application of the recursion relations gives the response functions at frequencies $\omega_j = \Omega\eta^j$, where j is the number of iterations. For a given Ω, this gives results only at widely separated frequencies. In order to sample the entire frequency range, the iterations are repeated for a large set of seed frequencies between Ω and $\eta\Omega$. Typical results for the case $\Gamma = 1/\gamma = 3$ are shown in Fig. 2a. We have

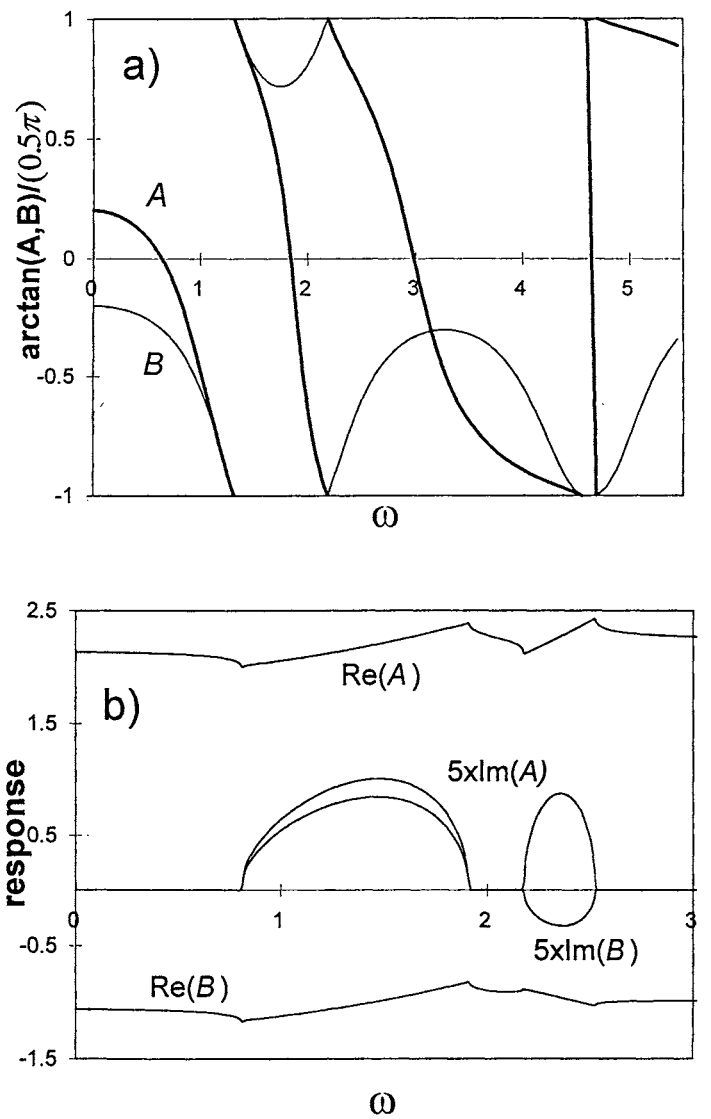

Fig. 2. (a): The frequency dependence of $\tan^{-1}(A(\omega))$ and $\tan^{-1}(B(\omega))$ which characterize the linear response of the Cantor set vibration model for $\Gamma = 1/\gamma = 3$ (b): The real and imaginary parts of the response functions $A(\omega)$ and $B(\omega)$ for the Sierpinski gasket vibration model for $\Gamma = \gamma = 1/10$. All curves are based on units where $k = m = 1$.

presented $\tan^{-1}(A(\omega))$ and $\tan^{-1}(B(\omega))$ in this figure, rather than the response functions themselves, only because the inverse tangent is a convenient way to represent functions with singularities.

The numerical results are relatively insensitive to the value of the response functions at the seed frequency. For example, with $\Omega = \omega_0/100$, no difference can be detected between the response functions obtained from $A(\Omega)$ and $B(\Omega)$ which are accurate to order Ω^2, and response functions obtained using the less accurate zero-order approximation; $A(\Omega) = -B(\Omega) = K$.

The singularities in the response functions represent normal modes of this Cantor-set model (with fixed end-points). The recursion relations tell us that ω^* is a normal-mode frequency, either because $A(\omega^*/\eta) - m(\omega^*/\eta)^2 = 0$ (so Eq. (6) is divergent), or because $A(\omega^*/\eta) + 2k/\Gamma - m(\omega^*/\eta)^2 = 0$ (so Eq. (7) is divergent). Also, using continuity, the recursion relations can be applied even at ω^* because singular terms in the numerator and denominator cancel—yielding a result which can be expressed in terms of the response functions at the lower frequency, ω^*/η. Thus a normal mode at ω^* means neither ω^*/η nor $\eta\omega^*$ are normal mode frequencies. In practice, numerical iterations of the recursion relations will occasionally land at frequencies which are very close to a normal mode frequency. To avoid the numerical problems which can occur when this happens, one can change to a second-order iteration of the recursion relations whenever the denominator in Eq. (6) or Eq. (7) becomes dangerously small.

Since $B(\omega)$ is non-zero, forces are transmitted across the Cantor set. However, at high frequencies $B(\omega)$ is extremely small except when the frequency approaches one of the normal mode frequencies.

The average distribution of normal mode frequencies can be obtained from the recursion relations. Let $N(\omega)$ be the total number of normal modes with frequency less than ω. ($N(\omega)$ is the integrated density of states.) The number of normal modes in the frequency range $\tilde{\omega} < \omega < (\tilde{\omega} + \Delta\omega)$ is thus $N(\tilde{\omega} + \Delta\omega) - N(\tilde{\omega})$, and the number of modes in the scaled frequency interval $\eta\tilde{\omega} < \omega < \eta(\tilde{\omega} + \Delta\omega)$ is $N(\eta(\tilde{\omega} + \Delta\omega)) - N(\eta\tilde{\omega})$. As will be shown below, the recursion relations tell us that the number of normal modes in the scaled interval is twice the number of normal modes in the original interval. Thus (changing notation so $\tilde{\omega}$ is replaced by ω)

$$\frac{N(\eta(\omega + \Delta\omega) - N(\eta\omega)}{N(\omega + \Delta\omega) - N(\omega)} \cong 2 \tag{8}$$

Writing the integrated density of states as

$$N(\omega) \cong \omega^p f(\omega) \tag{9}$$

and picking $\Delta\omega$ so that $\omega + \Delta\omega = \eta\omega$ gives a recursion relation for $f(\eta^n\omega)$ at different n. These recursion relations simplify and the factor of 2 is eliminated if we take

$$p = \frac{\ln(2)}{\ln(\eta)}. \tag{10}$$

Then letting $G_n = f(\eta^{n+1}\omega) - f(\eta^n\omega)$, Eq. (8) is equivalent to $G_{n+1} = G_n/2$. The resulting vanishing of the G_n for large n means that for large frequency, the function $f(\omega)$ is neither growing nor shrinking, but it is periodic in the log of its argument ($f(\eta\omega) \to f(\omega)$). This means the integrated density of states is characterized by a power law, but it is modulated by a function which is periodic in $\log(\omega)$ and does not approach a constant value. The power-law describing the density of states is valid only in the sense that $|\ln(N(\omega)) - p\ln(\omega)|$ is bounded, but it does not vanish as $\omega \to \infty$. This follows by taking the log of $N(\omega) \cong \omega^p f(\omega)$. The significant excursions of $N(\omega)$ away from its power-law approximation represent a clustering of normal mode frequencies.

To show that the number of normal modes really is doubled when the frequency interval is scaled by η, consider the nth and $(n+1)$th normal modes with frequencies ω_n and ω_{n+1}. As is shown in Fig. 2a, $A(\omega) - m\omega^2$ decreases continuously from $+\infty$ to $-\infty$ as the frequency increases from ω_n to ω_{n+1}. This means there is one frequency in this interval where the first recursion relation (Eq. (6)) is singular, and there is a different frequency where the second recursion relation (Eq. (7)) is singular. These singularities signify two normal modes in the scaled frequency range $\eta\omega_n < \omega < \eta\omega_{n+1}$. Of course one should not have to rely on Fig. 2a to show that $A(\omega) - m\omega^2$ is a decreasing function of frequency. A formal demonstration follows from the recursion relations. At very small frequencies we can use the power series expansions to show that both $F(\omega) = A(\omega) - m\omega^2 + B(\omega)$ and $G(\omega) = A(\omega) - m\omega^2 - B(\omega)$ have negative derivatives. Then taking a derivative of the recursion relations shows that the derivatives of $F(\eta^n\omega)$ and $G(\eta^n\omega)$ remain negative when the frequency is scaled by any power of η.

The response functions $A(\omega)$, $B(\omega)$ which characterize the Cantor set model can also be used to describe the vibrations of a one-dimensional lattice of these Cantor set models. In the Cantor-set lattice, a mass m with displacement X_n is both the left end of Cantor set number $n+1$ and the right end of Cantor set number n. Phonon propagation on this lattice corresponds to no applied force at site n, so using the response matrix,

$$0 = (2A(\omega) - m\omega^2)\, X_n + B(\omega)(X_{n+1} + X_{n-1}). \tag{11}$$

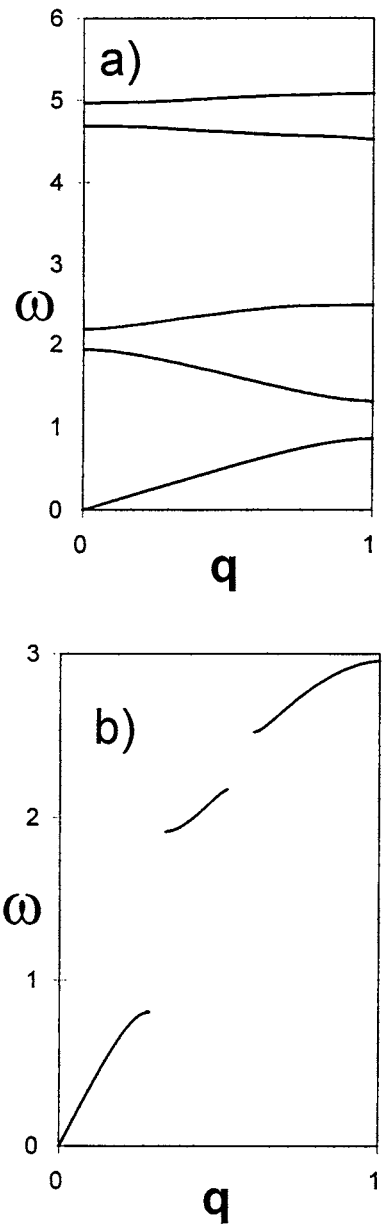

Fig. 3. (a): The lowest four branches of the phonon dispersion relations for the one-dimensional lattice of Cantor sets. Again, $\Gamma = 1/\gamma = 3$. (b): The phonon dispersion relation for the triangular lattice of Sierpinski gaskets. Gaps appear at frequencies where energy is absorbed by the gaskets. Again, $\Gamma = \gamma = 1/10$.

Seeking plane-wave solutions to Eq. (11) of the form $X_n = X_0 \exp(i\pi qn)$ determines the phonon's wave vector q in terms of its frequency ω. The resulting four lowest frequency branches of the phonon dispersion relations, again for the case $\Gamma = 1/\gamma = 3$, are shown in Fig. 3a. The sound velocity associated with the acoustic branch is the same as the sound velocity of a lattice of "atoms" in which the atomic mass is the total mass of one Cantor set, M, and the effective spring constant is given in terms of the static compressibility of the Cantor set, K. Increasingly high frequency branches of the phonon spectrum become increasingly narrow, and they converge to the normal-mode frequencies of a single Cantor set. This reflects the near-localization of the higher frequency normal modes of this model.

Finally, we note again that our characterization of the spectrum as a set of isolated points applies only when $\Gamma > 2$ and $\gamma < 1/2$, which corresponds to the case of finite total mass ($M < \infty$) and non-zero overall compressibility ($K > 0$). The same model is also well-defined when $1 < \Gamma < 2$ and $1/2 < \gamma < 1$. However, since the vibration spectrum for this second region of parameter space extends down to zero frequency, we cannot assume that the response functions are "smooth" near zero frequency, and this means a simple numerical application of the recursion relations is not possible.

3. SIERPINSKI GASKET MODEL

Different physical results can be obtained when our analysis is applied to more complex fractal-like systems, as is illustrated here by a model which is roughly related to the Sierpinski gasket.

The model is constructed by an infinite sequence of modifications of a triangle. Masses m are placed on the vertices of an equilateral triangle. They are coupled by three identical springs with spring constant k. For the second step, three smaller masses γm are placed at the center of each leg of the triangle, and these are connected to each other and to the two near vertices of the original triangle by nine springs with a weaker spring constant, Γk. The iteration procedure for this construction is illustrated in Fig. 1c. Each vertex of the gasket-like structure described here is connected to an infinite number of springs. In order for the model to make physical sense, the spring constants must become increasingly weak with each iteration, which means $\Gamma < 1$.

Like the Cantor set model of Section 2, this model is characterized by a frequency scaling parameter, η. Unlike the Cantor set model, $\eta = \sqrt{\Gamma/\gamma}$ need not be greater than unity. As will be shown below, $\eta = 1$ is a specially interesting case because the vibration spectrum becomes continuous. Note

that the scale-invariance of the characteristic frequencies means the spring constants and masses scale by the same amount, so their ratio does not change. The $\eta = 1$ case of our model is quite different from the Sierpinski gasket model described by Domany *et al.* and Rammal.

Vibrations of this Sierpinski gasket example are derived following arguments similar to those used for the Cantor set. Forces applied to the corners of the gasket are related to the vibration amplitudes at these corners by two response functions. Viewing the gasket on an expanded scale means the response can be written in terms of the response functions for the three sub-triangles.

The forces on the corners are denoted F, G, H, and the corresponding displacements are X, Y, Z. Symmetry means the inverse linear response matrix is again characterized by two linear response functions;

$$\begin{pmatrix} F \\ G \\ H \end{pmatrix} = \begin{pmatrix} A(\omega) - m\omega^2 & B(\omega) & B(\omega) \\ B(\omega) & A(\omega) - m\omega^2 & B(\omega) \\ B(\omega) & B(\omega) & A(\omega) - m\omega^2 \end{pmatrix} \begin{pmatrix} X \\ Y \\ Z \end{pmatrix}. \tag{12}$$

The forces and displacements at the midpoints on each edge opposite X, Y, Z. are denoted P, Q, R, and U, V, W. The inverse linear response matrix for all six coordinates and the corresponding forces is

$$\begin{pmatrix} F \\ G \\ H \\ P \\ Q \\ R \end{pmatrix} = \begin{pmatrix} \alpha_1 & -k & -k & 0 & b & b \\ -k & \alpha_1 & -k & b & 0 & b \\ -k & -k & \alpha_1 & b & b & 0 \\ 0 & b & b & \alpha_2 & b & b \\ b & 0 & b & b & \alpha_2 & b \\ b & b & b & b & b & \alpha_2 \end{pmatrix} \begin{pmatrix} X \\ Y \\ Z \\ U \\ V \\ W \end{pmatrix}. \tag{13}$$

Here

$$\alpha_1 = a(\omega) - m\omega^2 + 2k, \tag{14}$$

and

$$\alpha_2 = 2a(\omega) - \gamma m\omega^2. \tag{15}$$

The functions $a(\omega), b(\omega)$ are the scaled versions of $A(\omega), B(\omega)$, and Eqs. (3), (4) apply without alteration.

The recursion relations for the response functions are obtained by comparing the 6×6 matrix of Eq. (13) with the 3×3 matrix of Eq. (12).

Setting $P=Q=R=0$ in Eq. (12) means the forces are applied only at the corners of the triangle. When $P=Q=R=0$, the displacements at the midpoints of the sides (U, V, W) can be written in terms of the displacements at the corners (X, Y, Z). Then the forces at the corners are determined by the displacements at the corners, and the relationship between (F, G, H) and (X, Y, Z) derived from Eq. (13) must be the same as that given by Eq. (12).

Symmetric coordinates simplify the algebra. For F, G, and H, let

$$F_0=\frac{1}{\sqrt{3}}(F+G+H), \tag{16a}$$

$$F_+=\frac{1}{\sqrt{3}}(F+zG+z^*H), \tag{16b}$$

$$F_-=F_+^*, \tag{16c}$$

where $z=-1/2+i\sqrt{3}/2$. Analogous definitions apply for $X, Y, Z\rightarrow X_0, X_+, X_-$, $P, Q, R\rightarrow P_0, P_+, P_-$, and $U, V, W\rightarrow U_0, U_+, U_-$. Using these coordinates and forces, Eq. (12) becomes

$$\begin{pmatrix} F_0 \\ F_+ \\ F_- \end{pmatrix}=\begin{pmatrix} A(\omega)-m\omega^2+2B(\omega) & 0 & 0 \\ 0 & A(\omega)-m\omega^2-B(\omega) & 0 \\ 0 & 0 & A(\omega)-m\omega^2-B(\omega) \end{pmatrix}\begin{pmatrix} X_0 \\ X_+ \\ X_- \end{pmatrix} \tag{12'}$$

The four 3×3 blocks of Eq. (13) are similarly diagonalized using these coordinates. Thus the 6×6 matrix reduces to three 2×2 blocks. Two of these blocks are:

$$\begin{pmatrix} F_0 \\ P_0 \end{pmatrix}=\begin{pmatrix} a(\omega)-m\omega^2 & 2b(\omega) \\ 2b(\omega) & a(\omega)-\gamma m\omega^2+2b(\omega) \end{pmatrix}\begin{pmatrix} X_0 \\ U_0 \end{pmatrix}. \tag{13a}$$

and

$$\begin{pmatrix} F_+ \\ P_+ \end{pmatrix}=\begin{pmatrix} a(\omega)-m\omega^2+3k & -b(\omega) \\ -b(\omega) & 2a(\omega)-\gamma m\omega^2-b(\omega) \end{pmatrix}\begin{pmatrix} X_+ \\ U_+ \end{pmatrix}. \tag{13b}$$

The "+" and "−" systems have the same matrix, so the third 2×2 block gives no additional information. To relate the 2×2 block of Eq. (13a) to the first matrix diagonal matrix element of the symmetrized

3×3 matrix (Eq. 12')), we set $P_0 = 0$ (forces are only applied at the corners). This gives

$$U_0 = \frac{-2b(\omega)}{2a(\omega) - \gamma m\omega^2 + 2b(\omega)} X_0. \tag{17}$$

Using this expression for U_0 in Eq. (13a) gives a linear relation between F_0 and X_0. Comparing this result with Eq. (12'), and using the scaling relations between $a(\omega)$, $b(\omega)$ and $A(\omega)$, $B(\omega)$ gives one of two recursion relations;

$$A(\eta\omega) + 2B(\eta\omega) = \Gamma\left(A(\omega) - \frac{2(B(\omega))^2}{A(\omega) + B(\omega) - m\omega^2/2}\right). \tag{18}$$

Essentially the same algebra applies for Eq. (13b) and the second diagonal matrix element of Eq. (12'). Setting $P_+ = 0$ in Eq. (12b) gives

$$U_+ = \frac{b(\omega)}{2a(\omega) - \gamma m\omega^2 - b(\omega)} X_+, \tag{19}$$

which yields the second recursion relation for the response functions;

$$A(\eta\omega) - B(\eta\omega) - 3k = \Gamma\left(A(\omega) - \frac{(B(\omega))^2}{2A(\omega) - B(\omega) - m\omega^2}\right). \tag{20}$$

As with the Cantor set, physical results can be obtained from the recursion relations (Eqs. (18), (20)), provided Γ and γ are chosen so that the response functions are smooth and well-defined at low frequencies. The results for $\eta > 1$ show a sequence of normal-mode poles in the response functions which are qualitatively similar to the normal-mode structure of the Cantor-set model described earlier. However, the discrete normal mode spectrum changes to a continuous spectrum when the frequency-scaling parameter η is unity. Then Eqs. (18), (20) become simple second-order algebraic equations for the response functions $A(\omega)$, $B(\omega)$. The solutions to these equations show none of the singular structure associated with isolated normal modes. Instead, the response functions are smooth (but complex-valued) functions of the frequency, indicating a continuous vibration spectrum. The real and imaginary parts of both response functions for $\Gamma = \gamma = 1/10$ are shown in Fig. 2b. The two frequency ranges where the density of states is non-zero correspond to damped translation-like and compression-like vibrations.

It is indeed curious that when our model exhibits a scale invariance which is superficially similar to the characteristics of the Sierpinski gasket model studied by Rammal and Domany *et al.* (R–D), our conclusions

about the nature of the spectrum are completely different. Our continuous spectrum has absolutely no similarity to the highly degenerate "super-localized" normal mode spectrum of the R–D model. However, it should be remembered that our scale invariance results from canceling effects. Both springs and masses get smaller as one examines the system on a finer scale, and only a characteristic frequency $\omega = \sqrt{k/m}$ is unchanged. In contrast, every site and every spring in the R–D model is identical, and there are no long-ranged forces. Modes are "super-localized" in the R–D model because amplitudes cancel at sites surrounding a localized vibration, and this cancellation is much more difficult to achieve if there are long-ranged interactions and sites with differing masses.

As with the Cantor set, phonons can propagate on a triangular lattice of these Sierpinski gaskets. The phonon dispersion relations are again obtained from the response functions. For the case of phonon wave vectors perpendicular to the base of the triangles, the "no-force" condition gives

$$0 = 3A(\omega) - m\omega^2 + 2B(\omega)(1 + 2\cos(\pi q)). \tag{21}$$

Real values for the wave vector q are only obtained when the response functions are real. The gaps in the phonon dispersion curves of Fig. 3b (for $\Gamma = \gamma = 1/10$) correspond to frequency ranges where the individual Sierpinski gaskets absorb energy.

In conclusion, we have combined a hierarchy of physical attributes with the self-similarity of fractal geometry to produce soluble models of fractal vibrations. Our models exhibit different universality classes of spectra which result from variations of a material parameter, such as η. Various applications and extensions of this work are possible. The results apply as well to electric-circuit analogies of the mechanical systems. The linear response technique can be applied to fractal models in higher dimensions and to vector-valued vibrations amplitudes. There are also unresolved questions. For example, for some physically reasonable choices of the parameters Γ and γ, we cannot deduce the nature of the vibrations. Also, for the Sierpinski gasket, we believe the transition from the discrete to the continuous spectrum occurs at $\eta = 1$. Setting $\eta = 1 + \varepsilon$ yields an expansion in ε with singular properties. However, the simplicity of the recursions relations suggest that these equations could be a useful model for the study of the transition between different spectral types.

ACKNOWLEDGMENT

This work was supported in part by National Science Foundation Grant DMR 9023541. We acknowledge useful discussions with Professors J. Percus and A. Grosberg.

REFERENCES

1. Y. Gefen, B. B. Mandelbrot, and A. Aharony, *Phys. Rev. Lett.* **45:**855 (1980).
2. T. Nakayama, K. Yakubo, and R. L. Orbach, *Rev. Mod. Phys.* **66:**381 (1994).
3. M. Kohmoto, L. P. Kadanoff, and C. Tang, *Phys. Rev. Lett.* **50:**1870 (1983).
4. S. Ostlund, R. Pandit, D. Rand, H. J. Schellnhuber, and E. D. Siggia, *Phys. Rev. Lett.* **50:**1873 (1983).
5. B. Sutherland and M. Kohmoto, *Phys. Rev.* **B36:**5877 (1987).
6. M. Moulopoulos and S. Roch, *Phys. Rev.* **B53:**212 (1996).
7. G. Gumbs, G. S. Dubey, A. Salmon, B. S. Mahmoud, and D. Huang, *Phys. Rev.* **B52:**210 (1995).
8. H. Hiramoto and M. Kohmoto, *Int. J. Mod. Phys.* **B6:**281 (1992).
9. Y. Hu, D.-C. Tian, and L. Wang, *Phys. Lett.* **A207:**293 (1995).
10. F. Piechon, *Phys. Rev. Lett.* **76:** 4371 91996).
11. A. Hof, O. Knill, and B. Simon, *Commun. Math. Phys.* **174:**149 (1995).
12. W. P. Keirstead, H. A. Ceccato, and B. A. Huberman, *J. Stat. Phys.* **53:**733 (1988).
13. P. Kappertz, R. F. S. Andrade, and H. J. Schellnhuber, *Phys. Rev.* **B49:**14711 (1994).
14. F. Cracium *et al.*, *Phys Rev. Lett.* **68:**1444 (1992); *Phys. Rev.* **B49:**15067 (1994).
15. R. Rammal, *Journal de Physique* **45:**191 (1984).
16. E. Domany, S. Alexander, D. Benisimon, and L. P. Kadanoff, *Phys. Rev.* **B28:**3110 (1983).
17. B. W. Southern and A. R. Douchout, *Phys. Rev. Lett.* **55:**966 (1985).
18. K. Yakubo, *Phys. Rev.* **B42:**1078 (1990).
19. X. R. Wang, *Phys. Rev.* **B51:**9310 (1995).
20. D. J. Bergman and Y. Kantor, *Phys. Rev. Lett.* **53:**511 (1984).
21. P. J.-M. Monceau and J.-C. S. Levy, *Phys. Rev.* **B49:**1026 (1994).
22. W. A. Schwalm, C. C. Reese, C. J. Wagner, and M. K. Schwalm, *Phys. Rev.* **B49:**15650 (1994).
23. C. S. Jayanthi and S. Y. Wu, *Phys. Rev.* **B50:**897 (1994).
24. J. Q. You, C.-H. Lam, F. Nori, and L. M. Sander, *Phys. Rev.* **E48:** 4183 (1993).
25. F. S. de Menezes and A. C. N. de Magalhaes, *Phys. Rev.* **B46:**11642 (1992); see also the extensive references in this paper.